SMOV Report V: FOS Plate Scale and Orientation

A. Koratkar, T. Wheeler, I. Evans, O. Lupie, C. Taylor, C. Keyes, and A. Kinney
Space Telescope Science Institute

Instrument Science Report CAL/FOS--123
May, 1994

ABSTRACT

Plate scale factors for the FOS blue and red detectors are measured for the first time after COSTAR installation from the SMOV proposal ID number 5626 data. The analysis indicates that the scale factors are 1.258″ ± 0.014″ per diode height and 0.309″ ± 0.004″ per diode width for the blue detector, and 1.299″ ± 0.043″ per diode height and 0.301″ ± 0.003″per diode width for the red detector. The SMOV predictions were 1.232″ per diode height and 0.305″ per diode width for the blue detector and 1.232″ per diode height and 0.304″ per diode width for the red detector. The plate scales are not identical in the FOS X and Y directions because of the asymmetric magnification in the COSTAR X, Y meridional axes.

Mean rotation angles of 170°.6 and 97°.4 are measured between the nominal FOS Y axis and the V3 axis for the blue and red detectors respectively. The PDB will be updated after the results of the engineering tests determine the YPITCH value for each of the detectors.

1. INTRODUCTION

The insertion of COSTAR in the FOS light path not only causes the image to rotate (leading to a change of the angle between the FOS X, Y coordinate axes and the V2, V3 axes), but also causes a small distortion of any telescope scan pattern in the FOS detector plane. This distortion is caused by the asymmetric magnification in the COSTAR X, Y meridional axes. The effect of this asymmetric magnification is manifested as different plate scales for the FOS X and Y axes, and distortion of a square scan pattern into a rhombus.

1.1 Calculation of the expected scan pattern

Let the relative orientations of the V2, V3, FOS X, Y, and the COSTAR X_C, Y_C coordinate frames be as shown in Figure 1. Let θ be the rotation angle of the FOS X, Y axes relative to the V2, V3 axes; α the rotation angle of the COSTAR X_C, Y_C axes relative to the V2, V3 axes; and β the rotation angle of the COSTAR X_C, Y_C axes relative to the FOS X,Y axes. ABCD is the square that is transformed from the V2, V3 reference frame into the COSTAR X_C, Y_C reference frame. Next the correct magnification (m = B′D′/AC) is applied to ABCD, which transforms the figure into AB′CD′. AB′CD′ is then transformed from the COSTAR X_C, Y_C reference frame to the FOS X,Y reference frame to determine the expected distortion of the square scan pattern due to the presence of COSTAR.

From Figure 1 we see that any point P can be transformed into the various coordinate systems as follows:

$$\begin{bmatrix} V2 \\ V3 \end{bmatrix} = \begin{bmatrix} \cos\theta & \sin\theta \\ -\sin\theta & \cos\theta \end{bmatrix} \begin{bmatrix} X \\ Y \end{bmatrix}$$

where V2 and V3 are the coordinates of the point P in the V2, V3 reference frame; X and Y are the coordinates in the FOS X, Y frame; and θ is the rotation angle between the FOS X,Y and V2, V3 coordinate frames. The expected angle θ is 171°.8102 for the blue detector, and 98°.1898 for the red detector.

$$\begin{bmatrix} X_C \\ Y_C \end{bmatrix} = \begin{bmatrix} -\cos\alpha & \sin\alpha \\ \sin\alpha & \cos\alpha \end{bmatrix} \begin{bmatrix} V2 \\ V3 \end{bmatrix}$$

where V2 and V3 are the coordinates of the point P in the V2, V3 reference frame; X_C and Y_C are the coordinates in the COSTAR X, Y frame; and α is the rotation angle between the COSTAR X, Y and V2, V3 coordinate frames. The expected angle α is 315° for both the red and blue detectors.

$$\begin{bmatrix} X \\ Y \end{bmatrix} = \begin{bmatrix} -\cos\beta & -\sin\beta \\ -\sin\beta & \cos\beta \end{bmatrix} \begin{bmatrix} X_C \\ Y_C \end{bmatrix}$$

where X and Y are the coordinates of the point P in the FOS X,Y reference frame; X_C and Y_C are the coordinates in the COSTAR X, Y frame; and β is the rotation angle between the COSTAR X, Y and FOS X, Y coordinate frames. The expected angle β is -143°.19 for the blue detector and -216°.81 for the red detector.

Further, from Figure 1 we see that the relative magnification in the COSTAR X and Y axes is such that

$$\frac{B'D'}{AC} = m$$

where the expected value of m, from COSTAR optics test is 1.042 for the blue detector and 1.036 for the red detector. Thus, a square (ABCD) in the V2, V3 reference frame gets distorted into a rhombus (AB´CD´) in the FOS X,Y reference frame due to the presence of COSTAR in the light path. Using the expected values for m shows that due to the introduction of COSTAR the 90° angles of the square change as follows: the angles A and B are 92°.4 and 87°.6 repectively, for the blue detector, and 92.0°and 88.0° repectively for the red detector. The rotation of the rhombus with respect to the FOS X axis, i.e., the angle between the side AD´ of the rhombus and the FOS X axis, is expected to be 80°.6 for the blue detector and 187.2° for the red detector. The expected rhombus and its orientation is compared with observations to determine the plate scale and orientation of the FOS X, Y axes with respect to the V2, V3 axes. Further, the observations are used also to determine the relative magnification along the COSTAR X and Y axes.

2. OBSERVATIONS

The astrometric star NGC-188-255 in the NGC 188 astrometric field was observed with the FOS on 29th March 1994 and 31st March 1994 with both the blue and red detectors respectively to determine the precise plate scale of the FOS detectors. The sequence of observations conducted for each detector was as follows: (1) The target was acquired using a binary acquisition; (2) A confirmatory acquisition image was obtained to determine the location of the target in the 4.3″ aperture; (3) A 5×5 peak-up sequence with the 0.3″ aperture and step size 0.18″ was conducted to center the target in the 4.3″ aperture with better accuracy; (4) A confirmatory acquisition image was obtained once again to determine the location of the target in the 4.3″ aperture; (5) Two sets of 5×3 step and dwell scans were then performed to cover the 4.3″ aperture. These scans are used to determine the plate scale; (6) The star was then brought back to the center of the 4.3″ aperture and an ACQ image was obtained to once again determine the position of the star in the aperture after the scans; (7) The detector was switched and an ACQ image of the 4.3″ aperture was obtained. This move was conducted to determine the relative aperture positions of the two FOS detectors. The observations were obtained using IMAGE mode and the camera mirror. The high voltage for these observations was 22.2kv for the redside observations and 23.3kv for the blueside observations. FN format telemetry was used during the scans so that maximum number of FGS encoder readings (40 samples/second) of the guide star positions are available for each dwell point. Of the above observations only the two step and dwell scan sets will be discussed in this report. The rest of the data obtained will be discussed in another report.

3. ANALYSIS

3.1 Plate scale

The two sets of 5×3 step and dwell scans were performed as follows. The step sizes were 0.775″ or 1.55″ perpendicular to the array (Y-direction) and 0.775″ along the diode array (X-direction). The scan pattern for the two detectors is shown in Figure 2. Each image in the scan had 4 sub-steps per diode width and 64 Y-steps. Thus, each image has 152×64 pixels. The STSDAS tool APERLOCY is used to determine the stellar image center in measured FOS instrumental units.

The three methods used to locate the center are, 1) geometric midpoint, 2) flux centroid, and 3) cross correlation using a boxcar template. In the cross correlation technique, a 5×17 cross correlation template, which is the same size as the rectangular diode, is used to locate the aperture center. The centers determined by the flux centroid and the cross correlation technique are consistent within the measurement errors. The image centers determined by the cross correlation technique are used in the following analysis. The X and Y coordinates of each image center determined by the three techniques mentioned above are given in Table 1 and 2.

The corrected V2 and V3 positions from the FGS encoder for each observation were also calculated and the centroid of the jitter at each dwell point during the observation determined. The observations which had recentering events are marked in Figure 2 with parenthesis. Of these 5 dwell points with recentering events only two (y2b80109t and y2b80209t) had many recentering events occur during the dwell observation because of day and night transition. Further, we do not have corrected V2 and V3 positions for the dwell y2b8010yt. Next the dwell point seperations (in arcsec on the sky) in the X and Y direction in the two raster scans were calculated from the FGS astrometric calibration, and compared with the commanded offsets (see columns 2, 3 and 5 of Tables 3 and 4). Some offsets could not be calculated because FGS encoder readings for one of the observations is missing.

3.2 Orientation

The 30 observations used in the analysis form 6 roughly straight lines in the X-direction (along the diode array) and 10 lines in theY-direction (perpendicular to the diode array). See Figures 2. The orientation of the V2,V3 axes with respect to the FOS X, Y coordinate axes is calculated by determining the slopes of these 16 lines. The 16 lines in Table 5 are represented by the deflection points in each line. Table 5 also shows the slope of the line with respect to the FOS X axis.

4. RESULTS

4.1 Blueside Detector

Table 3 shows that an average X displacement of 0.775″ is executed when the telescope is commanded to offset 0.775″. The step sizes are accurate to <0.1% (or about .5 mas) in the X-direction. The average displacement (see Table 4) executed in the Y-direction was 0.775″ when commanded to offset 0.775″, and 1.55″ when commanded to offset 1.55″. The step sizes are accurate to < 0.1% (or about 0.3 mas) in the Y-direction.

The offsets determined by using APERLOCY (see columns 4 and 5, in Table 3 and 4) indicate that, in the Y-direction an average shift of 315.49 ± 3.01 ybases is seen when the telescope is commanded to offset 1.55″ ± 0.0005″, and 157.51 ± 0.88 ybases when commanded to offset 0.775″ ± 0.0003″. Similarly, in the X-direction an average shift of 2.503 ± 0.038 diodes is seen when commanded to offset 0.775″ ± 0.001″. These offsets indicate that the FOS blueside platescales are 0.0786″ ± 0.0006″/pixel and 0.0774″ ± 0.001″/pixel in the Y direction and the X direction respectively.
Binary target acquisition constraints require the effective diode height to correspond to 256 ybase units; and the FOS is configured to satisfy this constraint. This analysis indicates that a 1″ offset

produces an average shift of 203.50 ybase units. Hence, the measured effective diode height is 1.258″ ± 0.014″. The predicted SMOV value was 1.232″. The difference in the measured diode height, calculated from the present analysis and the predicted SMOV specifications, is 2.07%. This difference is 4.13 μm using a conversion factor of 0.781 μm/ybase (256 ybases = 200 μm). Since the diode response at the ends is not perfectly sharp and is affected by the conductors at the ends, the deviation in the effective diode height from the predicted is understood.

In the X-direction (along the diode array) this analysis indicates that a 0.309″ offset produces an average shift of 1 diode (see Table 3). The predicted SMOV scale factor indicated that a 0.305″ offset should produce a shift of 1 diode. The difference, calculated from the present analysis and the SMOV specifications, is 1.32%. This is a difference of 0.65 μm using a conversion factor of 50 μm/diode.

As discussed in the introduction section 1.1 and from Figures 1 and 2, since the plate scale is not perfectly identical in both the X and Y directions, the rectangular scan pattern on the sky is slightly skewed in the FOS detector space. The rhombus in Figure 2a. is such that the two parallel sides, have a mean rotation of -0°.18 ± 0°.40 and 87°.39 ± 0°.30 with respect to the X-direction. The angle formed by these two sides is 87°.57 ± 0°.5 corresponding to angle B in section 1.1. Also, from the discussion in section 1.1 we see that this angle corresponds to COSTAR magnification factor m =1.042, and the orientation of the rhombus with respect to the FOS X axis, for the magnification factor of 1.042 on the blueside, is determined to be 80.6°. The rotation angle between the V2, V3 axes and the FOS X, Y axes is 170°.6.

4.2 Redside Detector

For the redside detector an average X displacement of 0.775″ is executed when the telescope is commanded to offset 0.775″. The step sizes are accurate to within 0.12% (or about 1 mas) in the X-direction (see column 5 in Table 3). The average displacement executed in the Y-direction was 0.775″ when commanded to offset 0.775″, and 1.551″ when commanded to offset 1.55″. The step sizes are accurate to 0.12% (or about 1 mas) in the Y-direction (see column 5 in Table 4).

The offsets determined by using APERLOCY (see columns 6 Tables 3 and 4) indicate that, in the Y-direction an average shift of 305.17 ± 4.53 ybases is seen when the telescope is commanded to offset 1.551″ ± 0.002″, and 152.95 ± 6.45 ybases when commanded to offset 0.775″ ± 0.001″. Similarly, in the X-direction an average shift of 2.577 ± 0.026 diodes is seen when commanded to offset 0.775″ ± 0.001″. These offsets indicate that the FOS redside platescales are 0.0812″ ± 0.002″/pixel and 0.0752″ ± 0.0009″/pixel in the Y direction and the X direction, respectively.

A 1″ offset produces an average shift of 197.04 ybase units. Hence, the measured effective diode height is 1.299″ instead of the predicted value of 1.232″. The difference in the measured diode height, calculated from the present analysis and the predicted SMOV specifications, is 5.17%. This difference is 10.31 μm using a conversion factor of 0.781 μm/ybase unit. This deviation in the effective diode height from the predicted indicates that the value of the YPITCH (the engineering unit which constrains 256 ybase units = 200μm) has changed. Engineering tests have been scheduled to determine the value of YPITCH. With the present observations we predict that

the new redside YPITCH = 1.054 × the old YPITCH.

In the X-direction (along the diode array) this analysis indicates that a 0.301" offset produces an average shift of 1 diodes (see Table 3). The predicted SMOV scale factor indicated that a 0.304" offset should produce a shift of 1 diode. The difference, calculated from the present analysis and the SMOV specifications, is 1%. This is a difference of 0.50 μm using a conversion factor of 50 μm/diode.

The rhombus in Fig 2. is such that the two parallel sides, have a mean rotation of -0°.18 ± 0°.93 (excluding the lines 5-6-7-8-9 and k-l-m-n-o) and -88°.68 ± 0°.28 with respect to the X-direction. The angle formed by these two sides is 88°.5 ± 0°.97 corresponding to angle B in section 1.1. This angle corresponds to COSTAR magnification factor m=1.028 on the redside, and the orientation of the rhombus with respect to the FOS X axes on the redside is determined to be 187°.4. This indicates that the rotation angle between the V2, V3 axes and the FOS X, Y axes is 97°.4.

5. CONCLUSIONS

The plate scale and orientation for both the FOS detectors were determined. These values have not yet been updated in the PDB, because we are awaiting the results of an engineering test to determine the YPITCH for the detectors accurately.

Table 1: Stellar Image Centers from APERLOCY: Blueside

file name	x_midpoint (diodes)	y_midpoint (ybases)	x_centroid (diodes)	y_centroid (ybases)	x_crosscor (diodes)	y_crosscor (ybases)
y2b80105t	236.160	-1335.384	236.292	-1334.197	236.149	-1334.909
y2b80106t	238.639	-1335.122	238.694	-1333.496	238.628	-1334.138
y2b80107t	241.092	-1333.919	241.063	-1332.041	241.077	-1333.421
y2b80108t	243.574	-1330.523	243.474	-1328.664	243.556	-1330.491
y2b80109t	246.119	-1327.695	245.936	-1324.614	246.117	-1328.072
y2b8010at	246.415	-1015.782	246.229	-1015.422	246.418	-1015.612
y2b8010bt	243.897	-1017.625	243.846	-1017.363	243.899	-1016.513
y2b8010ct	241.373	-1018.080	241.377	-1018.627	241.368	-1016.862
y2b8010dt	238.822	-1016.972	238.878	-1016.750	238.796	-1015.713
y2b8010et	236.305	-1012.337	236.420	-1013.334	236.285	-1012.542
y2b8010ft	236.585	-697.149	236.759	-698.458	236.566	-696.748
y2b8010gt	239.071	-702.021	239.162	-704.477	239.060	-701.520
y2b8010ht	241.550	-703.503	241.549	-706.439	241.548	-704.078
y2b8010it	244.025	-702.357	243.983	-705.063	244.020	-702.068
y2b8010jt	246.506	-701.982	246.399	-703.853	246.503	-701.751
y2b8010kt	236.389	-1166.986	236.539	-1168.101	236.382	-1167.044
y2b8010lt	238.877	-1172.442	238.948	-1170.360	238.863	-1172.417
y2b8010mt	241.372	-1173.682	241.380	-1171.461	241.367	-1173.313
y2b8010nt	243.835	-1172.975	243.769	-1171.236	243.825	-1172.869
y2b8010ot	246.355	-1173.154	246.164	-1169.336	246.347	-1172.651
y2b8010pt	246.496	-1014.690	246.300	-1013.890	246.493	-1014.079
y2b8010qt	244.025	-1017.377	243.950	-1016.607	244.016	-1016.412
y2b8010rt	241.460	-1015.807	241.475	-1016.988	241.465	-1015.275
y2b8010st	238.910	-1013.845	238.980	-1014.665	238.908	-1013.635
y2b8010tt	236.392	-1009.658	236.511	-1010.304	236.390	-1010.058

Table 1: Stellar Image Centers from APERLOCY: Blueside

file name	x_midpoint (diodes)	y_midpoint (ybases)	x_centroid (diodes)	y_centroid (ybases)	x_crosscor (diodes)	y_crosscor (ybases)
y2b8010ut	236.596	-852.872	236.736	-856.568	236.579	-853.268
y2b8010vt	239.059	-858.534	239.137	-860.235	239.043	-857.385
y2b8010wt	241.568	-858.342	241.565	-861.401	241.561	-857.200
y2b8010xt	243.986	-859.448	243.969	-862.448	243.988	-859.069
y2b8010yt	246.538	-857.251	246.376	-858.387	246.530	-856.263

Table 2: Stellar Image Centers from APERLOCY: Redside

file name	x_midpoint (diodes)	y_midpoint (ybases)	x_centroid (diodes)	y_centroid (ybases)	x_crosscor (diodes)	y_crosscor (ybases)
y2b80205t	262.139	-557.993	262.217	-553.280	262.131	-556.925
y2b80206t	264.707	-557.837	264.771	-557.138	264.704	-558.535
y2b80207t	267.210	-557.787	267.165	-554.228	267.204	-557.488
y2b80208t	269.771	-549.744	269.681	-545.074	269.768	-548.866
y2b80209t	272.357	-545.990	272.264	-544.152	272.357	-546.165
y2b8020at	272.274	-243.633	272.115	-244.612	272.271	-243.998
y2b8020bt	269.697	-247.900	269.609	-248.032	269.692	-248.493
y2b8020ct	267.122	-253.141	267.095	-253.048	267.111	-253.012
y2b8020dt	264.525	-251.713	264.565	-251.776	264.528	-251.651
y2b8020et	261.917	-247.758	262.003	-249.576	261.918	-247.703
y2b8020ft	261.857	64.700	261.931	63.466	261.847	64.151
y2b8020gt	264.462	58.770	264.490	57.563	264.457	58.750
y2b8020ht	267.052	54.219	267.009	52.207	267.043	53.728
y2b8020it	269.604	52.303	269.520	50.311	269.591	51.310
y2b8020jt	272.164	56.014	272.027	54.787	272.162	55.754
y2b8020kt	261.991	-390.307	261.988	-389.026	261.990	-389.990
y2b8020lt	264.587	-397.557	264.622	-394.731	264.585	-397.068
y2b8020mt	267.194	-401.568	267.190	-399.831	267.192	-401.420
y2b8020nt	269.766	-404.927	269.698	-403.156	269.767	-404.609
y2b8020ot	272.332	-404.702	272.185	-403.911	272.322	-404.436
y2b8020pt	272.265	-241.653	272.102	-242.759	272.263	-242.199
y2b8020qt	269.667	-246.540	269.582	-246.635	269.669	-247.001
y2b8020rt	267.128	-248.719	267.103	-248.872	267.118	-248.736
y2b8020st	264.565	-249.762	264.597	-248.751	264.564	-248.673
y2b8020tt	261.954	-247.136	262.030	-249.292	261.953	-247.515

Table 2: Stellar Image Centers from APERLOCY: Redside

file name	x_midpoint (diodes)	y_midpoint (ybases)	x_centroid (diodes)	y_centroid (ybases)	x_crosscor (diodes)	y_crosscor (ybases)
y2b8020ut	261.895	-86.837	261.951	-88.289	261.894	-86.607
y2b8020vt	264.500	-91.815	264.537	-92.714	264.496	-91.928
y2b8020wt	267.063	-96.776	267.042	-97.659	267.059	-96.540
y2b8020xt	269.667	-97.209	269.601	-97.355	269.668	-96.614
y2b8020yt	272.232	-95.676	272.081	-97.886	272.230	-96.372

Table 3: Raster Scan Displacements in the X-Direction

Deflection Points	Commanded Shift (arcsec)	FGS Shift (arcsec)	Actual Shift (diodes)	FGS Shift (arcsec)	Actual Shift (diodes)
		Blueside		Redside	
5-6	0.775	0.774	2.47887	0.774	2.57230
6-7	0.775	0.775	2.44910	0.775	2.50070
7-8	0.775	0.776	2.47914	0.775	2.56400
8-9	0.775	0.776	2.56165	0.777	2.58862
a-b	0.775	0.773	2.51886	0.774	2.57837
b-c	0.775	0.773	2.53093	0.773	2.58121
c-d	0.775	0.775	2.57281	0.776	2.58267
d-e	0.775	0.774	2.51103	0.775	2.61063
f-g	0.775	0.774	2.49458	0.777	2.61002
g-h	0.775	0.774	2.48724	0.774	2.58643
h-i	0.775	0.778	2.47253	0.775	2.54758
i-j	0.775	0.773	2.48244	0.775	2.57089
k-l	0.775	0.777	2.48119	0.775	2.59521
l-m	0.775	0.773	2.50375	0.777	2.60742
m-n	0.775	0.774	2.45837	0.774	2.57434
n-o	0.775	0.777	2.52214	0.774	2.55548
p-q	0.775	0.773	2.47632	0.774	2.59360
q-r	0.775	0.773	2.55165	0.774	2.55054
r-s	0.775	0.775	2.55650	0.777	2.55441
s-t	0.775	0.775	2.51852	0.775	2.61108
u-v	0.775	0.774	2.46471	0.775	2.60159
v-w	0.775	0.776	2.51730	0.775	2.56317
w-x	0.775	-	2.42757	0.775	2.60904
x-y	0.775	-	2.54178	0.774	2.56219

Table 4: Raster Scan Displacements in the Y-Direction

Deflection Points	Commanded Shift (arcsec)	FGS Shift (arcsec)	Actual Shift (ybases)	FGS Shift (arcsec)	Actual Shift (ybases)
		Blueside		Redside	
5-e	1.55	1.550	322.367	1.552	309.222
6-d	1.55	1.549	318.425	1.552	306.883
7-c	1.55	1.550	316.5659	1.554	304.476
8-b	1.55	1.550	313.978	1.554	300.373
9-a	1.55	1.550	312.460	1.553	302.167
a-j	1.55	1.550	313.861	1.552	299.752
b-i	1.55	1.551	314.445	1.550	299.803
c-h	1.55	1.550	312.784	1.550	306.741
d-g	1.55	1.551	314.193	1.547	310.401
e-f	1.55	1.550	315.794	1.550	311.854
k-t	0.775	0.775	156.986	0.775	142.475
l-s	0.775	0.775	158.782	0.774	148.395
m-r	0.775	0.774	158.038	0.776	152.684
n-q	0.775	0.775	156.457	0.776	157.608
o-p	0.775	0.775	158.572	0.776	162.237
p-y	0.775	0.776	157.816	0.775	145.827
q-x	0.775	0.774	157.343	0.775	150.387
r-w	0.775	0.776	158.075	0.774	152.196
s-v	0.775	-	156.250	0.773	156.745
t-u	0.775	0.776	156.790	0.774	160.908

Table 5: Orientation with respect to the X-direction

Deflection points	Slope of Line (ybases/ diodes)	Θ (degrees)	Slope of Line (ybases/ diodes)	Θ (degrees)
	Blueside		Redside	
5-6-7-8-9	0.698	0.625	1.223	1.095
a-b-c-d-e	-0.272	-0.244	0.407	0.364
f-g-h-i-j	-0.426	-0.381	-0.943	-0.844
k-l-m-n-o	-0.469	-0.420	-1.411	-1.263
p-q-r-s-t	-0.428	-0.383	0.478	0.428
u-v-w-x-y	-0.307	-0.275	-0.937	-0.839
5-e-f	1468.40	87.504	-2014.60	-88.180
6-d-g	1437.18	87.450	-2362.00	-88.448
7-c-h	1312.17	87.208	-3766.94	-89.027
8-b-i	1257.01	87.085	-3364.65	-88.910
9-a-j	1470.56	87.508	-3074.64	-88.808
k-t-u	1240.60	87.047	-3136.63	-88.831
l-s-v	1611.79	87.726	-3148.69	-88.836
m-r-w	1633.62	87.756	-2279.61	-88.392
n-q-x	1200.07	86.947	-2381.96	-88.461
o-p-y	1555.92	87.645	-3280.93	-88.882

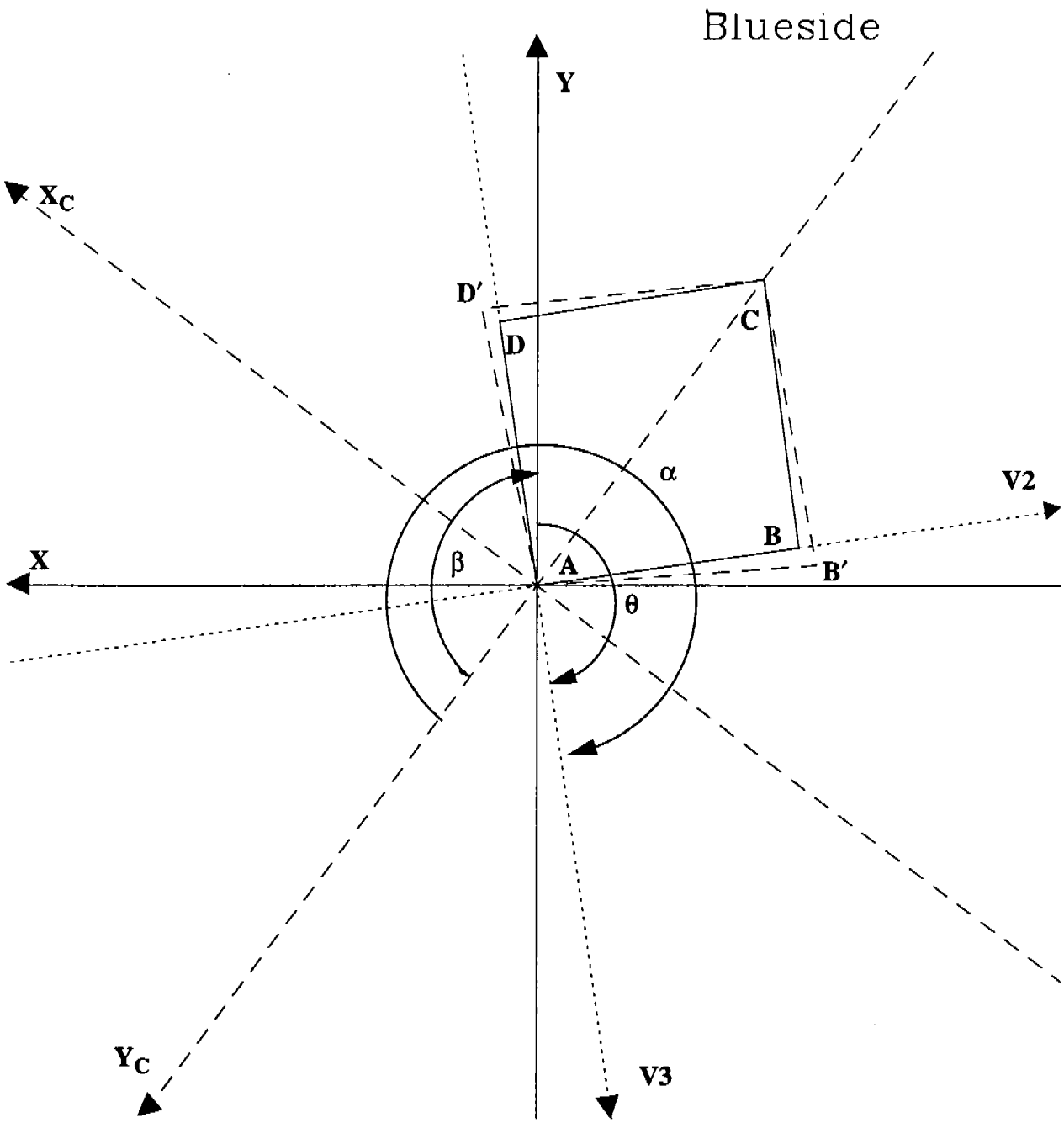

FIG--1a. The relative orientations of the V2, V3, FOS X, Y and the COSTAR X_C, Y_C co-ordinate frames for the blue detector. θ is the rotation angle of the FOS X, Y axes relative to the V2, V3 axes; α is the rotation angle of the COSTAR X_C, Y_C axes relative to the V2, V3 axes; and β is the rotation angle of the COSTAR X_C, Y_C axes relative to the FOS X,Y axes. The square ABCD is transformed form the V2, V3 reference frame into the COSTAR X_C, Y_C reference frame. Next the correct magnification (*m*) is applied to ABCD, which transforms the figure into AB′CD′. AB′CD′ is then transformed from the COSTAR X_C, Y_C reference frame to the FOS X, Y.

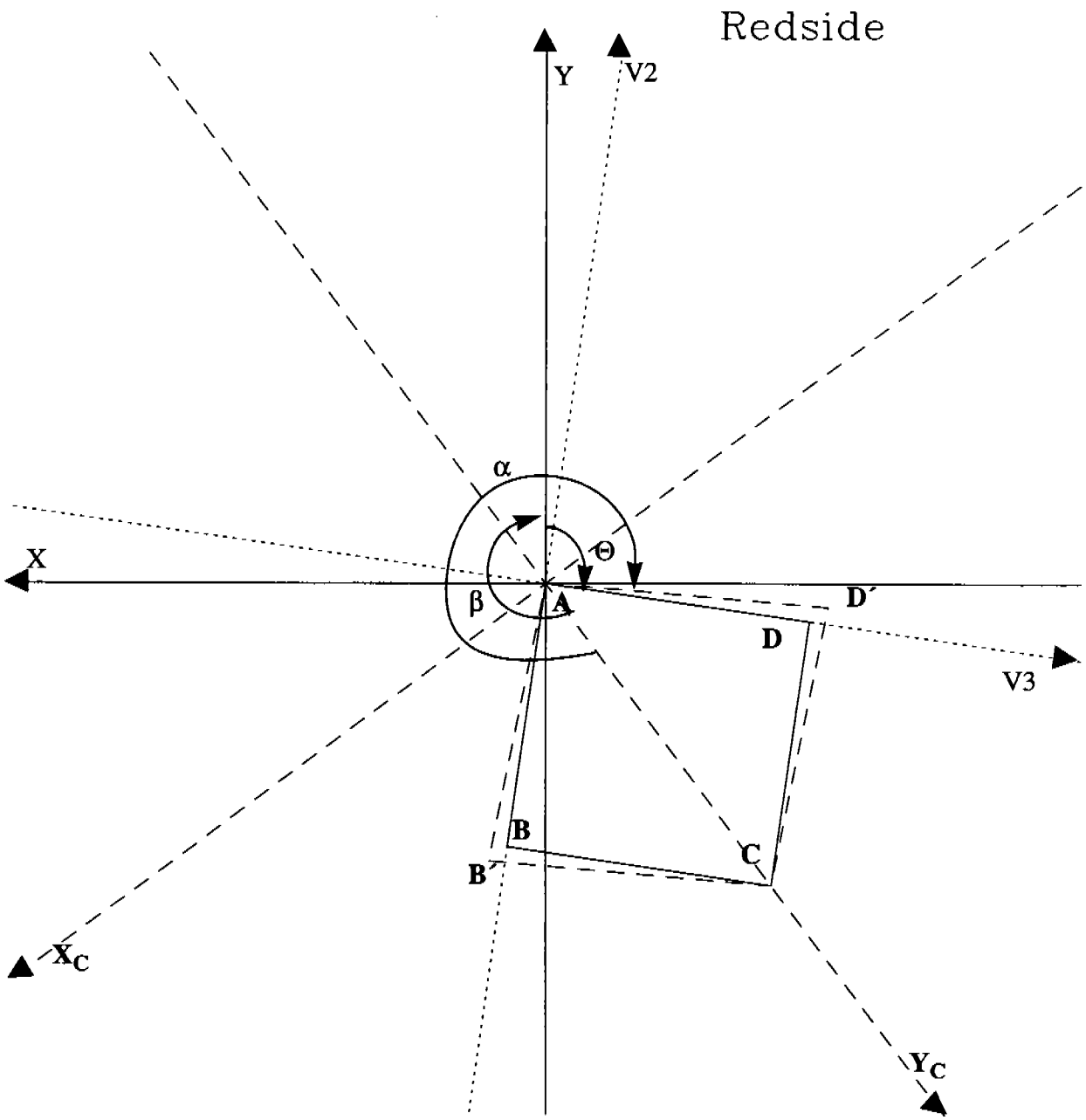

FIG--1b. Same as figure 1a for the red detector.

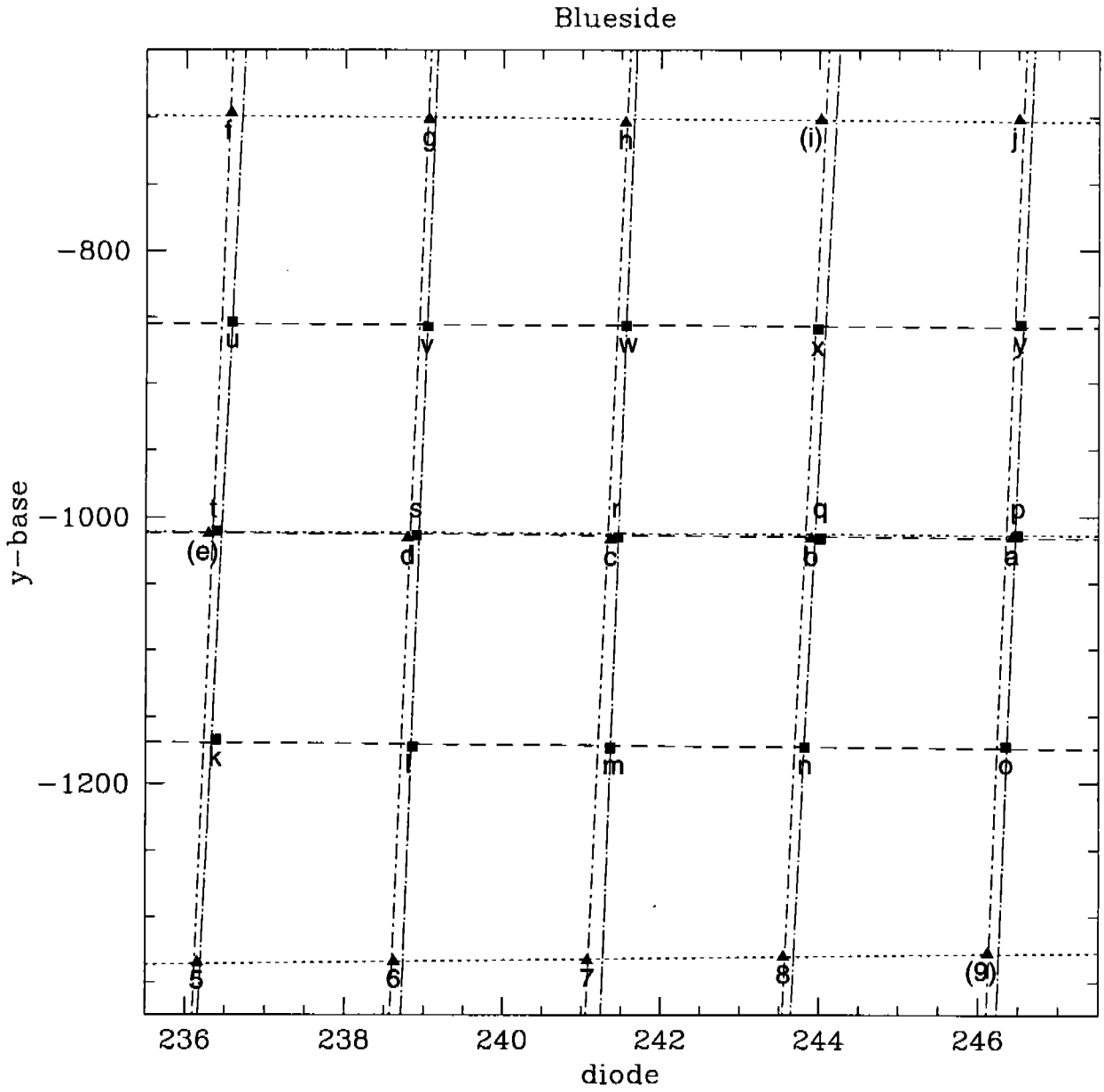

FIG--2a. The two scan patterns (solid line with triangles and dotted line with squares) are shown in FOS instrumental coordinates for the FOS blue detector. The 30 observations are identified by the next to last character from the image rootname in Table 1. The dwell points with recentering events are marked with parenthesis.

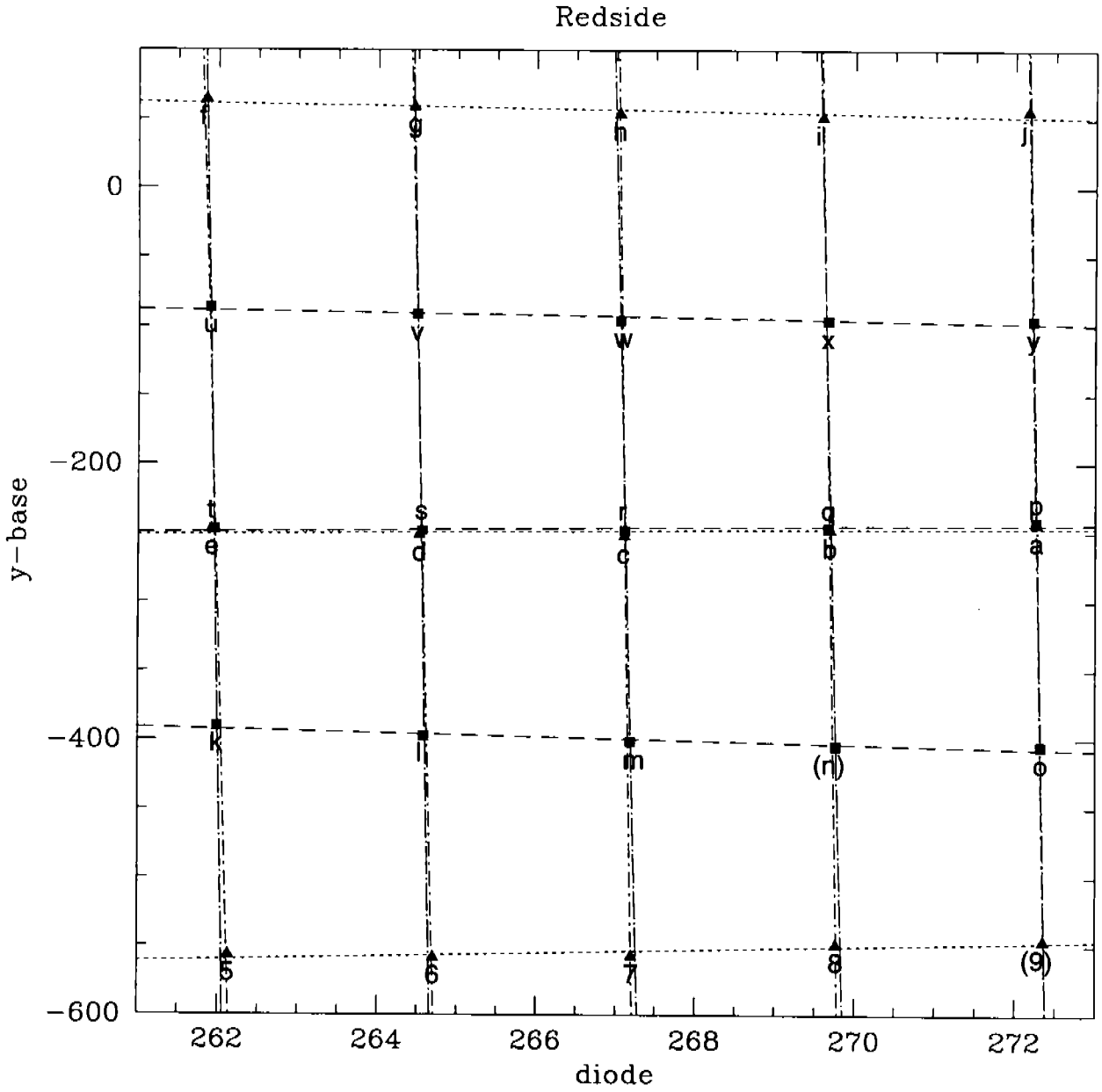

FIG--2b. Same as figure 1a for the red detector.